

# Saturating the quantum Cramér-Rao bound and measuring the related quantum Fisher information in a nitrogen-vacancy center in diamond

Yu Liu,<sup>1</sup> Min Yu,<sup>1</sup> Pengcheng Yang,<sup>1,\*</sup> Musang Gong,<sup>1</sup> Qingyun Cao,<sup>1</sup> Shaoliang Zhang,<sup>1</sup> Haibin Liu,<sup>1</sup> Markus Heyl,<sup>2</sup> Tomoki Ozawa,<sup>3,4</sup> Nathan Goldman,<sup>5,†</sup> and Jianming Cai<sup>1,6,‡</sup>

<sup>1</sup>*School of Physics, International Joint Laboratory on Quantum Sensing and Quantum Metrology, Huazhong University of Science and Technology, Wuhan 430074, China*

<sup>2</sup>*Max Planck Institute for the Physics of Complex Systems, Nöthnitzer Straße 38, Dresden 01187, Germany*

<sup>3</sup>*Advanced Institute for Materials Research, Tohoku University, Sendai 980-8577, Japan*

<sup>4</sup>*Interdisciplinary Theoretical and Mathematical Sciences Program (iTHEMS), RIKEN, Wako, Saitama 351-0198, Japan*

<sup>5</sup>*Center for Nonlinear Phenomena and Complex Systems, Université Libre de Bruxelles, CP 231, Campus Plaine, B-1050 Brussels, Belgium*

<sup>6</sup>*Wuhan National Laboratory for Optoelectronics,*

*Huazhong University of Science and Technology, Wuhan 430074, China*

(Dated: March 14, 2022)

The quantum Cramér-Rao bound sets a fundamental limit on the accuracy of unbiased parameter estimation in quantum systems, relating the uncertainty in determining a parameter to the inverse of the quantum Fisher information. We experimentally demonstrate near saturation of the quantum Cramér-Rao bound in the phase estimation of a solid-state spin system, provided by a nitrogen-vacancy center in diamond. This is achieved by comparing the experimental uncertainty in phase estimation with an independent measurement of the related quantum Fisher information. The latter is finely extracted from coherent dynamical responses of the system under weak parametric modulations, without performing any quantum-state tomography. Our method offers a versatile and powerful tool to explore the fundamental role of the quantum Fisher information in quantum technologies.

*Introduction.*— Quantum metrology has emerged as a key quantum technological application. It allows for the improvement of sensors performance, beyond any classically achievable precision, as was demonstrated in squeezed-light-based gravitational wave detectors [1]. According to the quantum Cramér-Rao bound, the accuracy of any unbiased estimation of an unknown system parameter is limited by the inverse of the quantum Fisher information (QFI) [2–7]. Importantly, the QFI only depends on the quantum state and is independent of the estimator; it is a geometric property of a quantum state in parameter space. Thus, for each parameter estimation problem, there potentially exists an optimal quantum measurement that saturates the Cramér-Rao bound. While such fully efficient estimators can be found for classical systems, it is challenging to identify an optimal quantum measurement scheme and to experimentally demonstrate the saturation of the quantum Cramér-Rao bound [8]. In particular, the experimental determination of the QFI is, in general, a complicated task [9–11]. Indeed, measuring the QFI requires, by definition, a very precise determination of the “distance” (fidelity) between two quantum states upon an infinitesimally small change of the system parameters [4, 5, 12].

In this work, we use a nitrogen-vacancy center in diamond to perform a fully efficient phase-estimation quantum measurement, which is shown to saturate the Cramér-Rao bound. In contrast to a previous study [8], where a saturation of the bound was identified through a theoretical estimation of the QFI, we perform an independent experimental measurement of the QFI within

our phase-estimation setting. This was achieved by probing spectroscopic responses upon weak parametric modulations, a technique which circumvents the stringent requirements of quantum-state tomography. Our method is inspired by a proposal to extract the quantum metric tensor [13, 14], which was recently implemented in NV centers [15] and superconducting qubits [16]. We demonstrate this approach in a Ramsey interferometer, which represents a standard experimental setting for the estimation of an unknown phase parameter. We determine the optimal sensitivity of the phase-parameter estimation through different resource states, and compare these results with their individual QFI.

*Experimental setting.*— In this work, we utilize a nitrogen-vacancy center (NV) in diamond as the quantum sensor. The ground state of the NV center spin has three spin sublevels  $m_s = \pm 1, 0$ . By applying an external magnetic field  $B_z \simeq 510$  G along the NV axis, we lift the degeneracy of the spin states  $m_s = \pm 1$  and use the two spin sublevels  $m_s = 0, -1$ , with states  $|0\rangle$  and  $|-\rangle$ , to form a quantum two-level system with an energy gap  $\omega_0 = D - \gamma_e B_z$ , where the zero-field splitting is  $D = (2\pi)2.87$  GHz and  $\gamma_e$  is the electronic gyromagnetic ratio [Fig.1(c)]. We use a microwave field to coherently manipulate the NV center spin state; see Fig.1(d) for an illustrative Rabi oscillation.

We perform a phase-parameter estimation measurement by means of Ramsey interferometry [Fig.1(a)]. For that purpose, we first initialize the system in a coherent superposition resource state,  $|\psi_\theta(0)\rangle = \cos(\theta/2)|0\rangle -$

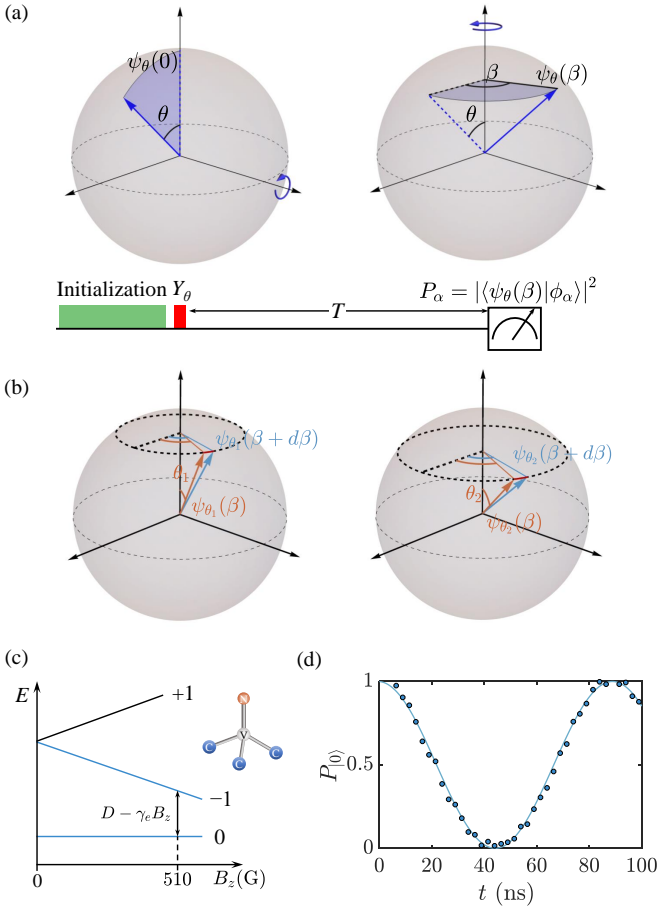


**FIG. 1. Experimental setting.** (a) Ramsey interferometry experiment for the estimation of an unknown phase parameter  $\beta$ . The quantum system is prepared in an initial resource state  $|\psi_\theta(0)\rangle$ , the evolution of which results in a phase parameter  $\beta$ . The measurement on the final state  $|\psi_\theta(\beta)\rangle$  allows to determine the value of the parameter  $\beta$ . (b) The QFI of the final state  $|\psi_\theta(\beta)\rangle$  reveals the information content relative to the unknown phase parameter  $\beta$ . The larger QFI (right) implies the better distinguishability between the states  $|\psi_\theta(\beta_0)\rangle$  and  $|\psi_\theta(\beta_0 + d\beta)\rangle$  that have an infinitesimal parametric difference  $d\beta \rightarrow 0$ . (c) The energy level structure of the NV center spin in diamond under an external magnetic field. The two-level quantum system is encoded by the ground state spin sublevels  $\{m_s = 0, -1\}$ . (d) Rabi oscillations: the population in the spin state  $m_s = 0$  as a function of time, which facilitates efficient coherent control of the NV center spin state.

$\sin(\theta/2)|-1\rangle$ , which we evolve into

$$|\psi_\theta(\beta)\rangle = \cos(\theta/2)|0\rangle - \sin(\theta/2)e^{i\beta}| -1\rangle, \quad (1)$$

according to the applied magnetic field. The phase parameter  $\beta$  of  $|\psi_\theta(\beta)\rangle$  can be estimated by performing positive-operator valued measurements (POVM) [5, 7],  $\mathcal{M} = \{\mathcal{M}_j\}$ ; as explained below, these are provided by spin-dependent fluorescence measurements [17]. The measurement precision is defined as the minimal change of the parameter  $\beta$  that can be detected from the con-

structed observable above the shot-noise level,

$$(\delta\beta)_{\mathcal{M}} = \Delta p / \left( \frac{\partial p}{\partial \beta} \right), \quad (2)$$

where  $p$  is the expectation value of the POVM signal,  $\Delta p$  is the uncertainty associated with the measurement signal. The fundamental limit of the achievable sensitivity of an unbiased estimator is given by the quantum Cramér-Rao bound [18–20]

$$\delta\beta \geq \frac{1}{\sqrt{\mathcal{F}_\beta}}, \quad (3)$$

where  $\mathcal{F}_\beta$  denotes the QFI, which for pure quantum states  $|\psi_\theta(\beta)\rangle$ , is given by [4, 5]

$$\mathcal{F}_\beta = 4 \left[ \langle \partial_\beta \psi(\beta) | \partial_\beta \psi(\beta) \rangle - |\langle \psi(\beta) | \partial_\beta \psi(\beta) \rangle|^2 \right]. \quad (4)$$

The QFI characterizes the distinguishability of adjacent quantum states over the parameter space [Fig.1(b)]. The purity of the states in our experiment, and hence the validity of Eq. (4) to capture the QFI, is discussed below. We note that the QFI is related to the real part of the quantum geometric tensor, which can be extracted through coherent dynamical responses [13, 15].

*Direct measurement of the QFI.*— It is one of the central goals of this work to show the saturation of the quantum Cramér-Rao bound through an independent experimental measurement of the QFI. We extract the QFI by probing coherent dynamical responses of the quantum system upon perturbative parametric modulations [13, 15]. Our measurement protocol is shown in Fig.2(a). The NV center spin is first initialized in the  $m_s = 0$  spin state by applying a green (532 nm) laser pulse, which also polarizes the nitrogen nuclear spin associated with the NV center as we tune the magnetic field close to the excited state level anticrossing (i.e.  $B_z \simeq 510$  Gauss). The subsequent microwave pulse, applied for a duration  $t_\theta = (\theta/\Omega)$ , rotates the NV center spin around the  $\hat{y}$  axis by an angle  $\theta$  according to the Hamiltonian  $H_1(t) = (\omega_1/2)\sigma_z + \Omega \cos(\omega_1 t)\sigma_x$ , where  $\omega_1$  matches the energy gap between the spin sublevels  $m_s = 0, -1$  and  $\Omega$  is the microwave Rabi frequency. The rotation, denoted as  $Y_\theta$ , prepares the NV center spin into the  $\theta$ -dependent resource state  $|\psi_\theta(0)\rangle$ . After the microwave pulse  $Y_\theta$ , the system undergoes a free evolution for a time  $T$ , according to an effective Hamiltonian  $H_2^{(e)} = [(\omega_0 - \omega_1)/2]\sigma_z$ , which results in the final state  $|\psi_\theta(\beta)\rangle$ ; see Eq (1). Here, the effective Hamiltonian  $H_2^{(e)}$  is defined in the interaction picture with respect to  $H_0 = (\omega_1/2)\sigma_z$ . The final state  $|\psi_\theta(\beta)\rangle$  encodes the information about the phase parameter  $\beta = \Delta T$  to be estimated, where  $\Delta = \omega_1 - \omega_0$ .

Inspired by the protocol of Ref. [13], we extract the QFI of the final state  $|\psi_\theta(\beta)\rangle$  by monitoring coherent transitions upon parametric modulations. This probing method requires the implementation of the following

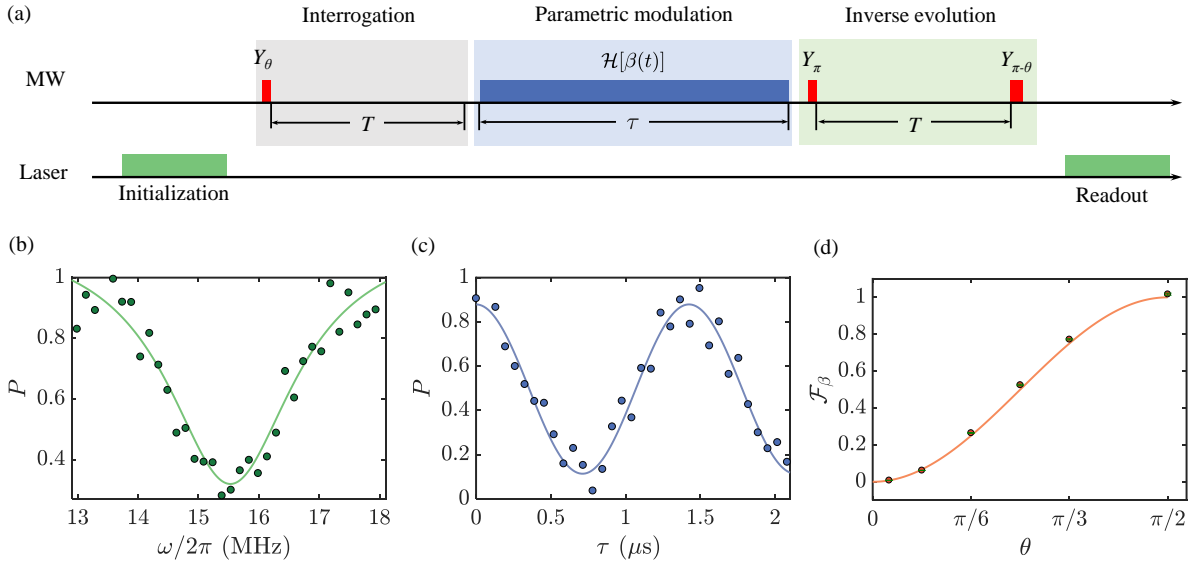


FIG. 2. **Direct measurement of the QFI.** (a) The pulse sequence for the measurement of the QFI using the NV center spin. The NV center spin is first polarized in the state  $|0\rangle$  by applying a green (532 nm) laser pulse and the  $\theta$ -dependent resource state  $|\psi_\theta(0)\rangle$  is prepared via a subsequent microwave pulse  $Y_\theta$ . The interrogation (i.e. the free evolution) for time  $T$  results in the parameter-dependent final state  $|\psi_\theta(\beta)\rangle$ . The parametric modulation via the amplitude and phase modulated microwave driving is described by the Hamiltonian  $H[\beta(t)]$ . The spin-dependent fluorescence after the inverse evolution, which rotates the state  $|\psi_\theta(\beta)\rangle$  back to the state  $|0\rangle$ , monitors the coherent transition probability induced by the parametric modulation. (b) The parameter modulation induced resonant transition measurement shows the probability that the NV center spin stays in the state  $|\psi_\theta(\beta)\rangle$  as a function of the modulation frequency  $\omega$  for a time  $\tau = 450$  ns. (c) shows the resonant coherent oscillation between the state  $|\psi_\theta(\beta)\rangle$  and  $|\psi_\theta^\perp(\beta)\rangle$  under parametric modulation. The other experiment parameters in (b) and (c) are  $\theta = \pi/3$ ,  $A = (2\pi)15.98$  MHz,  $a_\beta = 0.1$  and  $\Delta = (2\pi)5.025$  MHz. (d) The QFI measured in our experiment (red circle) is compared with the theoretical prediction (brown curve).

Hamiltonian

$$\mathcal{H}(\beta_0) = \frac{A}{2} \begin{pmatrix} \cos \theta & \sin \theta e^{-i\beta_0} \\ \sin \theta e^{i\beta_0} & -\cos \theta \end{pmatrix}, \quad (5)$$

such that the state  $|\psi_\theta(\beta)\rangle$  approximately corresponds to an eigenstate [17] of  $\mathcal{H}(\beta_0)$ . This is achieved by tuning the parameters of the microwave driving field acting on the NV center spin. The key step of our experiment then consists in generating parametric modulations [13]. To achieve this, we synthesize a microwave driving field with proper amplitude and phase modulations [15, 17], such that the “probing” Hamiltonian retains the form in Eq. (5), but with a time-periodic modulation of the parameter  $\beta_0$ , i.e.  $\mathcal{H}(\beta_0) \rightarrow \mathcal{H}(\beta_0 + a_\beta \cos(\omega t))$ .

The parametric modulation can induce a coherent transition from the state  $|\psi_\theta(\beta)\rangle$  to the other orthogonal eigenstate  $|\psi_\theta^\perp(\beta)\rangle$  of the Hamiltonian in Eq.(5) [13, 15]. This transition can be monitored by measuring the probability that the system remains in the state  $|\psi_\theta(\beta)\rangle$ . In the experiment, without requiring any prior information on the parameter  $\beta$ , we implement an inverse evolution sequence, consisting of two pulses ( $Y_\pi$  and  $Y_{\pi-\theta}$ ) separated by a free evolution of duration  $T$  [Fig.2(a)]. Such an inverse evolution rotates the states  $|\psi_\theta(\beta)\rangle$  and  $|\psi_\theta^\perp(\beta)\rangle$  back to the states  $|0\rangle$  and  $|1\rangle$ , respectively [17]. We then measure the population in state  $|0\rangle$ , which equals to the

sought population in state  $|\psi_\theta(\beta)\rangle$  after the application of the parametric modulation.

The efficiency of the coherent transition induced by the modulation is optimal whenever the modulation frequency matches the energy gap between the states  $|\psi_\theta(\beta)\rangle$  and  $|\psi_\theta^\perp(\beta)\rangle$ . In the experiment, we first perform the modulation-induced-transition measurement for a wide range of modulation frequencies, from which we determine the resonant modulation frequency  $\omega \simeq A$ ; see Fig.2(b). We then apply the parametric modulation at the resonant frequency, and measure the population in the state  $|\psi_\theta(\beta)\rangle$  as a function of the perturbation duration  $\tau$ ; see Fig.2(c). This data is fitted using a function  $P_0 = [1 + \cos(\nu_\theta t)]/2$ , which defines the effective Rabi frequency  $\nu_\theta$ . From this data, we extract the  $\theta$ -dependent QFI,  $\mathcal{F}_\beta(\theta)$ , using the relation [17]

$$\mathcal{F}_\beta(\theta) = 4 \left( \frac{\nu_\theta}{a_\beta \omega} \right)^2. \quad (6)$$

This experimental measurement of the QFI is displayed in Fig.2(d), which shows excellent agreement with the theoretical prediction  $\mathcal{F}_\beta = \sin^2 \theta$ . In particular, it clearly demonstrates the dependence of the QFI on the initial resource state  $|\psi_\theta(0)\rangle$ . The precision of our measurement relies on the accuracy of the engineered Hamiltonian  $\mathcal{H}(\beta_0)$  and on the determination of the effective Rabi

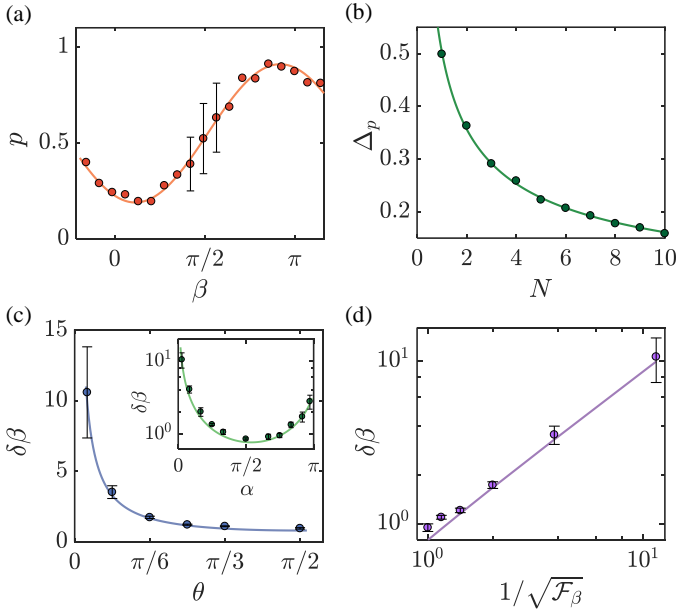


**FIG. 3. Saturating the quantum Cramér-Rao bound.** (a) The Ramsey interferometry measurement signal  $p = \langle S \rangle$ . The measurement data allows us to obtain the susceptibility  $\chi_\alpha = \partial p / \partial \beta$  of the measurement signal close to the working point  $\beta = \pi/2$ . The error bars represent the uncertainty of the parameter estimation  $\Delta p = [\langle S^2 \rangle - \langle S \rangle^2]^{1/2}$  with the number of repetitions  $N = 9$ . The parameters are  $\theta = \pi/3$ ,  $\alpha = \pi/2$ ,  $\Delta = (2\pi)2.27$  MHz and  $A = (2\pi)11.34$  MHz. (b) The uncertainty of the parameter estimation  $\Delta p$  as a function of the number of repetitions  $N$  can be fitted by a function of the form  $\Delta p = \Delta_0/\sqrt{N}$  (green curve). (c) The optimal measurement sensitivity  $\delta\beta$  (achieved by the projective measurement  $P_\alpha$  with  $\alpha = \pi/2$ ) by using different  $\theta$ -dependent resource states  $|\psi_\theta(0)\rangle$ . Inset: The sensitivity  $\delta\beta$ , achieved by applying the projective measurement  $P_\alpha$  as a function of  $\alpha$  when  $\theta = \pi/2$  and  $\beta = \pi/2$ , shows that the optimal measurement sensitivity in our Ramsey interferometry experiment is obtained when  $\alpha = \pi/2$ . (d) The linear relation  $\delta\beta \propto 1/\sqrt{\mathcal{F}_\beta}$ , where  $\mathcal{F}_\beta$  is the quantum Fisher information; the measured proportionality factor is  $1.041 \pm 0.036$ . The number of repetitions in (c-d) is  $N = 1$ . The curves in (a, c-d) are theoretical predictions.

frequency  $\nu_\theta$ . The imperfection in the interrogation step [Fig. 2(a)] may result in a mixed state rather than a pure state  $|\psi_\theta(\beta)\rangle$ ; this would decrease the contrast of the Rabi oscillations and affect the measurement accuracy. By reconstructing the density matrix through projective measurements, we estimate the state fidelity to be above 95% in our experiment [17], which is evidenced by the good agreement between our results and the theoretical predictions.

*Reaching the quantum Cramér-Rao bound.*— The QFI measurement enables us to experimentally show that our phase-parameter estimator exhibits optimal performance by saturating the quantum Cramér-Rao bound in Eq. (3). In order to analyze the relation between the measure-

ment precision and the QFI, we now determine the measurement sensitivity for the estimation of the parameter  $\beta$  within our Ramsey interferometry experiment. To do so, we first apply the rotation  $Y_\theta$  on the NV center spin qubit to prepare the initial state  $|\psi_\theta(0)\rangle$ . We tune the free evolution time such that the parameter  $\beta = \Delta T$  is close to the working point where the best sensitivity occurs, i.e.  $\beta \simeq \pi/2$  where the slope  $\partial p / \partial \beta$  is maximal [Fig. 3(a)]. To build an estimator of the parameter  $\beta$ , we apply a rotation  $Y_\alpha$ , which is equivalent to a projective measurement  $P_\alpha = |\phi_\alpha\rangle\langle\phi_\alpha|$  on the final state  $|\psi_\theta(\beta)\rangle$ , where  $|\phi_\alpha\rangle = \cos(\alpha/2)|0\rangle + \sin(\alpha/2)|-1\rangle$ . The observable of interest is then provided by the function  $p(\beta; \theta, \alpha) = \langle\psi_\theta(\beta)|P_\alpha|\psi_\theta(\beta)\rangle$ , from which we aim to estimate the parameter  $\beta$  with optimal accuracy [Eq (3)].

In our experiment, the observable  $p$  is extracted from the collected photons of a fluorescence signal [17]. Due to the limited collection efficiency, the signal photons are accumulated over many sweeps of an experimental sequence, which constitutes one experimental run of our measurement. In the  $j$ -th run, based on the photon number  $n_j$  detected from the rotated spin state  $Y_\alpha|\psi_\theta(\beta)\rangle$ , we assign a measurement value  $s_j = 1$  or 0 according to the probabilities  $p_j = (n_j - n_1)/(n_0 - n_1)$  and  $1 - p_j$ , where  $n_0$  and  $n_1$  are the average photon numbers obtained from the bare spin states  $m_s = 0$  and  $m_s = -1$ , respectively. This allows us to construct an observable  $S = (1/N) \sum_{j=1}^N s_j$ , whose expectation value yields [17] the desired function  $\langle S \rangle = p(\beta; \theta, \alpha)$ . The data obtained from repeated measurements [Fig. 3(a)] allows us to determine the slope of the signal, which is defined as  $\chi_\alpha = \partial p / \partial \beta = [p(\beta + d\beta) - p(\beta)]/d\beta$ . From the experimental data, we can also extract the measurement uncertainty  $\Delta p$  associated with the observable  $S$ ; see Fig. 3(b). We note that the uncertainty scales with the number of repetitions  $N$  as  $\Delta p = \Delta_0/\sqrt{N} + \xi_0$  [17]. The first term arises from the shot-noise with  $\Delta_0 = [p(1 - p)]^{1/2}$ , while the second term  $\xi_0$  represents the contribution from the systematic noise that cannot be averaged out.

We first compare the sensitivity  $\delta\beta = \Delta p / \chi_\alpha$  obtained by projective measurements over different bases  $P_\alpha$ . The experimental results shown in the inset of Fig. 3(c) demonstrate that the optimal measurement sensitivity is obtained when  $\alpha = \pi/2$ , which agrees with the theoretical prediction [17], since  $(\delta\beta)^2 = [1 - (\cos \beta \sin \theta)^2]/|\sin \beta \sin \theta|^2$ . The slight deviation arises from other sources (apart from shot noise). The measurement precision also depends on the angle  $\theta$  of the resource state  $|\psi_\theta(0)\rangle$ , which accounts for the QFI of the final state  $|\psi_\theta(\beta)\rangle$ : we proceed by determining the optimal measurement sensitivity with different resource states  $|\psi_\theta(0)\rangle$  in view of testing the quantum Cramér-Rao bound in Eq (3). It can be seen from the results shown in Fig. 3(c) that the optimal measurement sensitivity improves as the angle  $\theta$  approaches  $\pi/2$ , i.e. when the resource state  $|\psi_\theta(0)\rangle$  becomes a maximally coherent

superposition state. The optimal measurement sensitivity verifies the quantum Cramér-Rao bound (3), as finally demonstrated in Fig.3(d).

*Conclusions.* — By introducing an experimental technique to measure the QFI in a solid-state spin system, we have shown how Ramsey-based phase estimation can become fully efficient by saturating the quantum Cramér-Rao bound. The presented technique provides a versatile tool to explore the fundamental role of the QFI in various physical scenarios, including quantum metrology, but also entanglement properties of many-body quantum systems [14, 21] and the quantum speed limit in the context of optimal control [22–26].

*Acknowledgements.* — This work is supported by the National Natural Science Foundation of China (11874024, 11690032). T.O. is supported by JSPS KAKENHI Grant Number JP18H05857, JST PRESTO Grant Number JPMJPR19L2, JST CREST Grant Number JP-MJCR19T1, and the Interdisciplinary Theoretical and Mathematical Sciences Program (iTHEMS) at RIKEN. N.G. is supported by the ERC Starting Grant TopoCold and the Fonds De La Recherche Scientifique (FRS-FNRS) (Belgium). This project has received funding from the European Research Council (ERC) under the European Union’s Horizon 2020 research and innovation programme (grant agreement No. 853443), and M.H. further acknowledges support by the Deutsche Forschungsgemeinschaft via the Gottfried Wilhelm Leibniz Prize program.

P. Giorda, A. Meda, M. G. A. Paris, and A. Shurupov, Experimental estimation of entanglement at the quantum limit, *Phys. Rev. Lett.* **104**, 100501 (2010).

[9] H. Strobel, W. Muessel, D. Linnemann, T. Zibold, D. B. Hume, L. Pezzè, A. Smerzi, and M. K. Oberthaler, Fisher information and entanglement of non-Gaussian spin states, *Science* **345**, 424 (2014).

[10] Y. Li and W.-D. Li, Reasonable method to extract Fisher information from experimental data, *Physica A* **514**, 606 (2019).

[11] Y.-N. Lu, Y.-R. Zhang, G.-Q. Liu, F. Nori, H. Fan, and X.-Y. Pan, Observing information backflow from controllable non-Markovian multi-channels in diamond, *arXiv:1912.00845* (2019).

[12] L. Pezzè, Y. Li, W.-D. Li, and A. Smerzi, Witnessing entanglement without entanglement witness operators, *Proc. Natl. Acad. Sci. U.S.A.* **113**, 11459 (2016).

[13] T. Ozawa and N. Goldman, Extracting the quantum metric tensor through periodic driving, *Phys. Rev. B* **97**, 201117 (2018).

[14] T. Ozawa and N. Goldman, Probing localization and quantum geometry by spectroscopy, *Physical Review Research* **1**, 032019 (2019).

[15] M. Yu, P.-C. Yang, M.-S. Gong, Q.-Y. Cao, Q.-Y. Lu, H.-B. Liu, M. B. Plenio, F. Jelezko, T. Ozawa, N. Goldman, S.-L. Zhang, and J.-M. Cai, Experimental measurement of the complete quantum geometry of a solid-state spin system, *Natl. Sci. Rev.* **7**, 254 (2020).

[16] X.-S. Tan, D.-W. Zhang, Z. Yang, J. Chu, Y.-Q. Zhu, D.-Y. Li, X.-P. Yang, S.-Q. Song, Z.-K. Han, Z.-Y. Li, Y.-Q. Dong, H.-F. Yu, H. Yan, S.-L. Zhu, and Y. Yu, Experimental Measurement of the Quantum Metric Tensor and Related Topological Phase Transition with a Superconducting Qubit, *Phys. Rev. Lett.* **122**, 210401 (2019).

[17] See Supplemental Material for further experiment details, which includes Refs.[2, 3, 13, 15].

[18] C. W. Helstrom, ed., *Quantum Detection and Estimation Theory* (Academic, New York, 1976).

[19] A. Holevo, *Probabilistic and Statistical Aspects of Quantum Theory* (Springer, New York, 2011).

[20] M. Hayashi, Quantum Information Geometry and Quantum Estimation, in *Quantum Information Theory* (Springer, Berlin, Heidelberg, 2017) Chap. 6, p. 253.

[21] P. Hauke, M. Heyl, L. Tagliacozzo, and P. Zoller, Measuring multipartite entanglement through dynamic susceptibilities, *Nat. Phys.* **12**, 778 (2016).

[22] V. Giovannetti, S. Lloyd, and L. Maccone, Quantum limits to dynamical evolution, *Phys. Rev. A* **67**, 052109 (2003).

[23] M. M. Taddei, B. M. Escher, L. Davidovich, and R. L. de Matos Filho, Quantum Speed Limit for Physical Processes, *Phys. Rev. Lett.* **110**, 050402 (2013).

[24] A. del Campo, I. L. Egusquiza, M. B. Plenio, and S. F. Huelga, Quantum Speed Limits in Open System Dynamics, *Phys. Rev. Lett.* **110**, 050403 (2013).

[25] D. P. Pires, M. Cianciaruso, L. C. Céleri, G. Adesso, and D. O. Soares-Pinto, Generalized Geometric Quantum Speed Limits, *Phys. Rev. X* **6**, 021031 (2016).

[26] M. Kolodrubetz, D. Sels, P. Mehta, and A. Polkovnikov, Geometry and non-adiabatic response in quantum and classical systems, *Phys. Rep.* **697**, 1 (2017).

\* pengchengyang@hust.edu.cn

† ngoldman@ulb.ac.be

‡ jianmingcai@hust.edu.cn

[1] L. S. Collaboration, A gravitational wave observatory operating beyond the quantum shot-noise limit, *Nature Physics* **7**, 962 (2011).

[2] H. Cramér, *Mathematical Methods of Statistics* (Princeton University Press, Princeton, 1946).

[3] C. R. Rao, Information and the Accuracy Attainable in the Estimation of Statistical Parameters, in *Breakthroughs in Statistics: Foundations and Basic Theory* (Springer, New York, 1992) pp. 235–247.

[4] S. L. Braunstein and C. M. Caves, Statistical distance and the geometry of quantum states, *Phys. Rev. Lett.* **72**, 3439 (1994).

[5] S. L. Braunstein, C. M. Caves, and G. J. Milburn, Generalized Uncertainty Relations: Theory, Examples, and Lorentz Invariance, *Ann. Phys. (N.Y.)* **247**, 135 (1996).

[6] D. Petz and C. Ghinea, Introduction to quantum fisher information, in *Quantum Probability and Related Topics*, edited by R. Rebolledo and M. Orszag (World Scientific, Singapore, 2011) pp. 261–281.

[7] J. S. Sidhu and P. Kok, Geometric perspective on quantum parameter estimation, *AVS Quantum Science* **2**, 014701 (2020).

[8] G. Brida, I. P. Degiovanni, A. Florio, M. Genovese,

**Supplementary Material for**  
**Saturating the quantum Cramér-Rao bound and measuring the related**  
**quantum Fisher information in a nitrogen-vacancy center in diamond**

**S.1. Measurement of the Quantum Fisher information**

*1. The QFI and quantum Cramér-Rao bound*

In the general quantum parameter estimation experiment, the parameter  $\beta$  is usually encoded into a quantum resource state  $|\psi(\beta)\rangle$ . For a pure state  $|\psi(\beta)\rangle$ , the quantum Fisher information (QFI) is defined as follows

$$\mathcal{F}_\beta = 4 \left[ \langle \partial_\beta \psi(\beta) | \partial_\beta \psi(\beta) \rangle - |\langle \psi(\beta) | \partial_\beta \psi(\beta) \rangle|^2 \right]. \quad (\text{S.1})$$

The shot-noise limit sensitivity for the parameter estimation by constructing any parameter estimator is bounded by the reciprocal of the square root of the QFI, namely

$$\delta\beta \geq \frac{1}{\sqrt{\mathcal{F}_\beta}}. \quad (\text{S.2})$$

This is the celebrated quantum Cramér-Rao bound [1, 2].

*2. Experimental realization*

In the experiment, we utilize the NV center spin in diamond as a two-level quantum sensor to perform a Ramsey interferometry experiment for parameter estimation. The NV center spin is initialized to the spin state  $|0\rangle$  and then prepared into the state  $|\psi_\theta(0)\rangle = Y_\theta|0\rangle = \cos(\theta/2)|0\rangle - \sin(\theta/2)|-1\rangle$  by an unitary rotation  $Y_\theta = \exp(-i\theta\sigma_y/2)$ . The free evolution of the system for a time  $T$  is governed by the Hamiltonian  $H_s = \Delta\sigma_z/2$ , where  $\Delta$  represents a magnetic field. This results in the following state that contains the information on the parameter  $\beta = \Delta T$  as

$$|\psi_\theta(\beta)\rangle = e^{-i\beta H_s} |\psi_\theta(0)\rangle = \begin{bmatrix} \cos(\theta/2)e^{i\beta/2} \\ \sin(\theta/2)e^{-i\beta/2} \end{bmatrix} \quad (\text{S.3})$$

According to the definition in Eq.(S.1), the QFI of the state  $|\psi_\theta(\beta)\rangle$  with respect to the estimation of the parameter  $\beta$  is dependent on the initial resource state  $|\psi_\theta(0)\rangle$ , namely

$$\mathcal{F}_\beta = \sin^2 \theta. \quad (\text{S.4})$$

In order to measure the QFI of the state  $|\psi_\theta(\beta)\rangle$  directly, we first synthesize the microwave driving field

$$f_0(t) = (A \sin \theta) \cos [(\omega_1 - A \cos \theta)t + \beta], \quad (\text{S.5})$$

acting on the NV center spin, which leads to the effective Hamiltonian  $\mathcal{H}(\beta_0)$  as follows

$$\mathcal{H}(\beta_0) = \frac{A}{2} (\cos \beta_0 \sin \theta \sigma_x + \sin \beta_0 \sin \theta \sigma_y + \cos \theta \sigma_z). \quad (\text{S.6})$$

The parameters in the above Hamiltonian (Eq.S.6) are controllable through microwave engineering. In the experiment, we calibrate the above Hamiltonian by verifying that the state  $|\psi_\theta(\beta)\rangle$  is approximately its eigenstate, see Fig.S1. We proceed to implement in our experiment the following time-dependent Hamiltonian as

$$\mathcal{H}_{\text{eff}}[\beta(t)] = \mathcal{H}(\beta_0 + a_\beta \cos(\omega t)) \simeq H(\beta_0) + a_\beta \cos(\omega t) \partial_\beta \mathcal{H}(\beta)|_{\beta=\beta_0}, \quad (\text{S.7})$$

with the designed parametric modulation as follows

$$\beta = \beta_0 + a_\beta \cos(\omega t). \quad (\text{S.8})$$

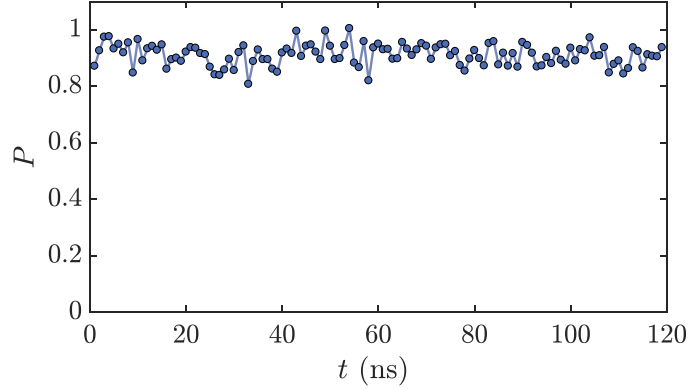


FIG. S1. Calibration of Hamiltonian engineering. The parameters in the Hamiltonian  $\mathcal{H}(\beta_0)$  (Eq.S.6) are tuned such that the state  $|\psi_\theta(\beta)\rangle$  is approximately its eigenstate. The plot shows the probability of the NV center spin staying in the state  $|\psi_\theta(\beta)\rangle$  as a function of the evolution time  $t$  when the system's dynamics is governed by the Hamiltonian  $\mathcal{H}(\beta_0)$  (Eq.S.6). The experimental parameters are  $A = (2\pi)15.79$  MHz,  $\theta = \pi/2$ ,  $\omega_1 = (2\pi)1440.6$  MHz and  $T \simeq 150$  ns.

We observe the resonant coherent transition between the eigenstates of the Hamiltonian  $\mathcal{H}(\beta_0)$  (Eq.S.6) induced by the parametric modulation, which is shown in Fig.2(b) in the main text. In this case, the parametric modulation frequency  $\omega = \omega_0$ , where  $\omega_0$  is the energy gap between the eigenstates. To measure the state  $|\psi_\theta(\beta)\rangle$  population after the parametric modulation for time  $\tau$  (the corresponding system's state is denoted as  $|\psi_{\theta,\beta}(\tau)\rangle$ ), we first implement an inverse evolution by  $Y_\pi$  and  $Y_{\pi-\theta}$  pulses with a free evolution for time  $T$  between these two pulses, see Fig.2(a) in the main text. Such an inverse evolution can be described by the following unitary transformation as

$$\hat{U} = Y_{\pi-\theta} \exp(-i\Delta\beta T \sigma_z) Y_\pi = Y_\theta^{-1} \exp(i\Delta\beta T \sigma_z) = [\exp(-i\Delta\beta T \sigma_z) Y_\theta]^{-1}, \quad (\text{S.9})$$

which realizes that  $\hat{U}|\psi_\theta(\beta)\rangle = |0\rangle$  and  $\hat{U}|\psi_\theta^\perp(\beta)\rangle = |-1\rangle$ . The subsequent spin-dependent fluorescence measurement  $\hat{P}_0 = |0\rangle\langle 0|$  is thus equivalent to the projective measurement  $\hat{P} = \hat{U}^\dagger |0\rangle\langle 0| \hat{U} = |\psi_\theta(\beta)\rangle\langle\psi_\theta(\beta)|$  on the state  $|\psi_{\theta,\beta}(\tau)\rangle$ . Therefore, we are able to monitor the state  $|\psi_\theta(\beta)\rangle$  population dynamics under resonant parametric modulation which can be described by  $P_\beta(t) = [1 + \cos(\nu_\theta t)]/2$ , where [3, 4]

$$\nu_\theta = (1/2)a_\beta\omega_0\sqrt{\mathcal{F}_\beta[\psi_\theta(\beta)]}. \quad (\text{S.10})$$

Therefore, we are able to determine the QFI of the state  $|\psi(\beta)\rangle$  as follows

$$\mathcal{F}_\beta[\psi_\theta(\beta)] = 4 \left( \frac{\nu_\theta}{a_\beta\omega_0} \right)^2. \quad (\text{S.11})$$

## S.2. Experiment details on the verification of quantum Cramér-Rao bound

### 1. Parameter estimation via Ramsey interferometry experiment

In our experiment, we perform quantum parameter estimation based on Ramsey interferometry, as shown in Fig.1(a) in the main text. The two-level quantum system is realized by the spin sublevels in the ground state manifold of the NV center, i.e.  $|m_s = 0\rangle$  and  $|m_s = -1\rangle$ . The system is coherently manipulated by microwave field pulses which are described by the following Hamiltonian

$$H_{\text{pulse}} = (\omega_1/2)\sigma_z + A \sin[(\omega_1 + \delta)t]\sigma_x, \quad t \in [t_0, t_0 + \tau_{\text{pulse}}], \quad (\text{S.12})$$

where  $\omega$  denotes the energy gap between the states  $|0\rangle$  and  $|-1\rangle$  when applying microwave field, and  $\tau_{\text{pulse}}$  represents the time duration for microwave pulse. We remark that the energy splitting of the spin sublevels may slightly change due to microwave driving. In the interaction picture with respect to  $H_0 = (\omega_1 + \delta)/2\sigma_z$ , we get the following effective

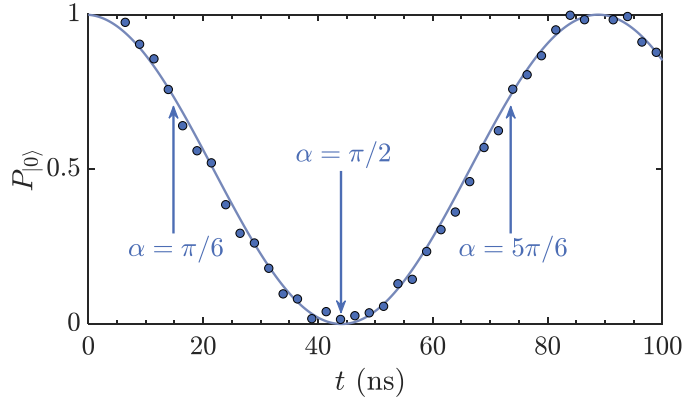


FIG. S2. Microwave pulse for the implementation of projective measurement. The projective measurement  $\hat{P}_\alpha = |\phi_\alpha\rangle\langle\phi_\alpha|$ , where  $|\phi_\alpha\rangle = \cos(\alpha/2)|0\rangle + \sin(\alpha/2)|-1\rangle$ , can be realized by an unitary rotation  $Y_\alpha = \exp(-i\alpha\sigma_y/2)$  before the spin-dependent fluorescence measurement. The red dots show the population of the state  $|0\rangle$  as a function of the microwave pulse duration, which allows to determine Rabi period  $T_{Rabi}$ . The rotation  $Y_\alpha$  can be realized by setting the microwave pulse duration time as  $\tau_\alpha = \alpha T_\alpha/\pi$ . As an example, we mark three microwave pulse duration times  $\tau_\alpha$  for  $\alpha = \pi/6, \pi/2, 5\pi/6$  in the figure.

Hamiltonians during the microwave pulses ( $H_I^{(1)}$ ) and the free evolution ( $H_I^{(0)}$ ) respectively

$$H_I^{(1)} = -\frac{\delta}{2}\sigma_z + \frac{A}{2}\sigma_y \quad (\text{S.13})$$

$$H_I^{(0)} = -\frac{\Delta}{2}\sigma_z \quad (\text{S.14})$$

with  $\Delta = \delta + (\omega_1 - \omega_0)$  where  $\omega_0$  denotes the energy gap between the states  $|0\rangle$  and  $| - 1\rangle$  during the free evolution.

In the experiment, the NV center spin is initialized to  $|0\rangle$  and then is prepared into the  $\theta$ -dependent resource state  $|\psi_\theta(0)\rangle$  by an unitary rotation  $Y_\theta = \exp(-i\theta\sigma_y/2)$  which is realized by applying a microwave pulse with a Rabi frequency  $\Omega$  for a time duration  $\tau_{pulse_1} = \theta/\Omega$ . Here, we remark that  $\delta \ll \Omega$ , thus the error in the rotation is negligible. The free evolution process (from  $\tau_{pulse_1}$  to  $\tau_{pulse_1} + T$ ) leads to a dynamical phase accumulation given by the parameter  $\beta = \Delta T$ , and the system evolves to the following final state as

$$|\psi(\theta, \beta)\rangle = \exp(i\Delta T\sigma_z/2)Y_\theta|0\rangle = \cos(\theta/2)e^{-i\beta/2}|0\rangle - \sin(\theta/2)e^{i\beta/2}| - 1\rangle. \quad (\text{S.15})$$

The second unitary rotation  $Y_\alpha = \exp(i\alpha\sigma_y/2)$  to implement the projective measurement  $\hat{P}_\alpha$ , is realized by a microwave pulse for a time duration  $\tau_{pulse_2} = \alpha/\Omega$ , see Fig. S2, implements the projective measurement  $\hat{P}_\alpha = |\phi_\alpha\rangle\langle\phi_\alpha|$  where  $|\phi_\alpha\rangle = \cos(\alpha/2)|0\rangle + \sin(\alpha/2)| - 1\rangle$ . In the experiment, we choose the free evolution time  $T$  such that the working point is close to  $\beta \simeq \pi/2 + k\pi$  where the measurement signal exhibits the maximum slope.

In additional, we reconstruct the prepared state according to the measurement results  $p(\beta; \theta, \alpha) = \text{Tr}\{\rho(\beta; \theta)\hat{P}_\alpha\}$  from a set of 11 different projective measurements  $\hat{P}_\alpha$ . By performing the following minimization procedure as

$$\text{Min}_{\{r, \theta_e, \phi_e\}} \left\{ \sum_\alpha \left[ \text{Tr}\{\rho^R(r, \theta_e, \phi_e)\hat{P}_\alpha\} - p(\beta; \theta, \alpha) \right]^2 \right\}, \quad (\text{S.16})$$

wherein  $\rho^R(r, \theta_e, \phi_e) = 1/2[\mathbb{1} + r(\sin \theta_e \cos \phi_e \sigma_x + \sin \theta_e \sin \phi_e \sigma_x + \cos \theta_e \sigma_z)]$ , we can get the most likely density matrix  $\rho$  for the prepared state. As an example, our estimation suggests a state preparation fidelity of  $F = 96.2\%$  fidelity in Fig. S3 with  $F = \langle\psi(\theta, \beta)|\rho(\beta; \theta)|\psi(\theta, \beta)\rangle$ .

## 2. Quantum parameter estimation protocol

The sensitivity of quantum parameter estimation is dependent on the measurement protocol. In the experiment, we perform projective measurement on the NV center spin that is described by the operator  $\hat{P}_\alpha = |\phi_\alpha\rangle\langle\phi_\alpha|$  with the basis state  $|\phi_\alpha\rangle = \cos(\alpha/2)|0\rangle + \sin(\alpha/2)| - 1\rangle$ . We count the number of photons in the first 300 ns of the laser pulse

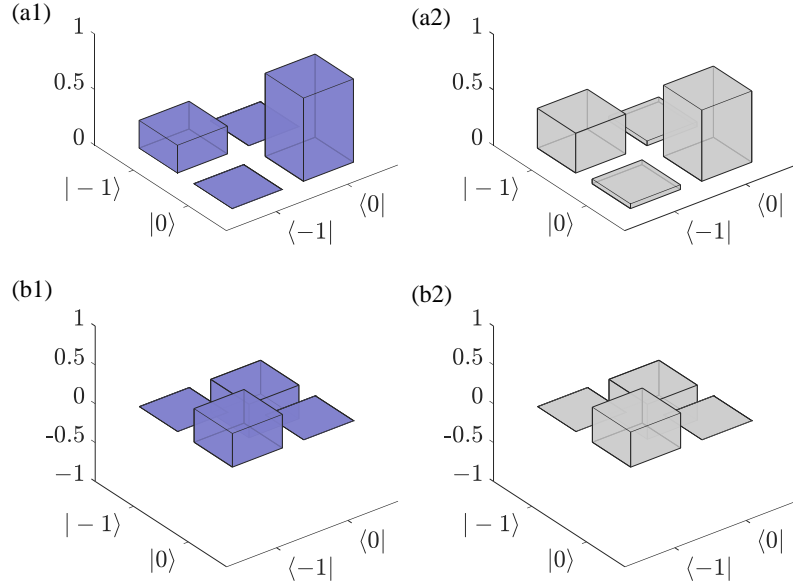


FIG. S3. State preparation fidelity. We plot the density matrix elements of the prepared state  $\rho$  based on the results from a set of different projective measurements  $\hat{P}_\alpha$ , which are compared with the ones of the ideal state  $|\psi(\theta, \beta)\rangle\langle\psi(\theta, \beta)|$ . The four panels show the real (a1, a2) and imaginary (b1, b2) parts of the density matrices, wherein the blue bars show the ideal state and the solid gray bars show the density matrix of the estimated prepared state. The fidelity is estimated to be  $F = 96.2\%$ , which is defined as  $F = \langle\psi(\theta, \beta)|\rho(\beta; \theta)|\psi(\theta, \beta)\rangle$ . The parameters are  $\theta = \pi/3$  and  $\beta = \pi/2$ .

as the signal photons. Due to the limit of collection efficiency, the signal photons are accumulated over a number of sweeps of an experimental measurement sequence, which constitutes one experiment run of measurement. We denote the averaged photon number obtained from the bare spin state  $m_s = 0$  and  $m_s = -1$  as  $n_0$  and  $n_1$  respectively. We introduce a variable  $s = 1/0$  to represent the spin state  $m_s = 0/m_s = -1$ . For the NV center spin system, the signal photons are spin-dependent, namely  $(n_0 - n_1)/n_0 \simeq 30\%$ , see Fig.S4(a). For a quantum state  $\rho$  with the state  $|0\rangle$  population  $p = \langle 0|\rho|0\rangle$ , the number of photons  $n_j$  collected in the  $j$ -th experiment run fluctuates and follows the distribution  $n_j \sim p\mathcal{N}(n_0, \sigma_0^2) + (1 - p)\mathcal{N}(n_1, \sigma_1^2)$ , see an example shown in Fig.S4(b). According to the number of signal photons  $n_j$ , we assign a measurement value  $s_j = 1$  or 0 according to the probabilities  $p_j = (n_j - n_1)/(n_0 - n_1)$  and  $1 - p_j$ . This allows us to construct an observable  $S = (1/N) \sum_{j=1}^N s_j$ , the expectation value of which is

$$\langle S \rangle = \frac{1}{N} \langle \sum_{j=1}^N s_j \rangle = \langle p_j \rangle = p(\beta; \theta, \alpha) \quad (\text{S.17})$$

The variance of the observable  $S$  is given by

$$\begin{aligned} (\Delta s)^2 &= \langle S^2 \rangle - \langle S \rangle^2 \\ &= \langle \left[ \frac{1}{N} \sum_j^N (s_j - p) \right]^2 \rangle \\ &= \frac{1}{N^2} \left\langle \sum_{j=1}^N s_j^2 + \sum_{j \neq k}^N s_j s_k - 2Np \sum_{j=1}^N s_k + N^2 p^2 \right\rangle \\ &= \frac{1}{N} (\langle s_j^2 \rangle - p^2) \\ &= \frac{p(1 - p)}{N}. \end{aligned}$$

We note that

$$p = \frac{1}{2} (1 + \cos \theta \cos \alpha - \sin \theta \sin \alpha \cos \beta), \quad (\text{S.18})$$

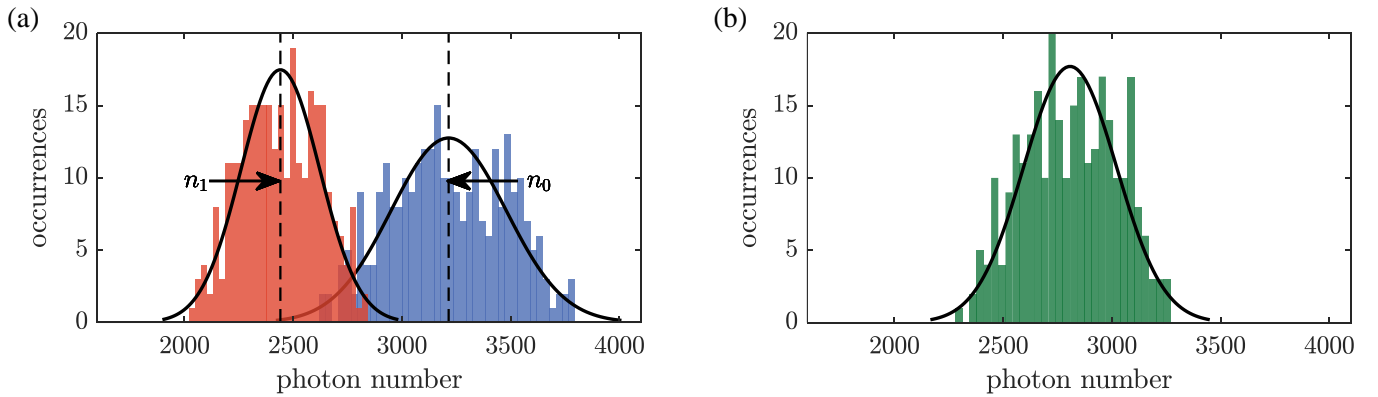


FIG. S4. (a) shows the histogram of the number of photons collected from the spin state  $| -1 \rangle$  (red) and  $| 0 \rangle$  (blue) with the averaged number of photons  $n_1$  and  $n_0$  respectively. (b) shows the histogram of the number of photons collected while the NV center spin is in the superposition state  $| + \rangle = (1/\sqrt{2})(| 0 \rangle + | -1 \rangle)$ .

thus we can construct the following estimator for the parameter  $\beta$  as

$$\check{\beta} = \arccos \left( \frac{1 + \cos \theta \cos \alpha - 2S}{\sin \theta \sin \alpha} \right) \quad (\text{S.19})$$

$$= \arccos \left[ \frac{1}{\sin \theta \sin \alpha} \left( \cos \theta \cos \alpha - \frac{N_0 - N_1}{N} \right) \right], \quad (\text{S.20})$$

where  $N_0$  and  $N_1$  represents the number of  $s_j = 0$  and 1 respectively. With  $\alpha = \pi/2$ , the estimator becomes

$$\check{\beta} = \arccos \left[ \frac{1}{\sin \theta} \left( \frac{N_1 - N_0}{N} \right) \right]. \quad (\text{S.21})$$

The precision can be written as

$$\delta \beta = \frac{\Delta s}{\left| \partial_{\langle \hat{S} \rangle} \hat{\beta} \right|} = \frac{2\Delta s}{|\sin \theta \sin \alpha \sin \beta|} \quad (\text{S.22})$$

which gives the optimal sensitivity with  $\alpha = \pi/2$  satisfying the quantum Cramér-Rao bound.

### 3. Optimal measurement to achieve quantum Cramér-Rao bound

In our experiment, we perform projective measurement on the state  $|\psi_\theta(\beta)\rangle = \cos(\theta/2)e^{-i\beta/2}|0\rangle - \sin(\theta/2)e^{i\beta/2}| -1 \rangle$  to estimate the value of the parameter  $\beta$ . We compare the measurement sensitivity achieved by different projective measurements, which are described by  $\hat{P}_\alpha = |\phi_\alpha\rangle\langle\phi_\alpha|$  with  $|\phi_\alpha\rangle = \cos(\alpha/2)|0\rangle + \sin(\alpha/2)| -1 \rangle$ . The measurement signal obtained from different projective measurements are shown in Fig. S5. Following the protocol as presented in the above section, we analyze the variance of parameter estimation and thereby obtain the measurement sensitivity from the projective measurement  $\hat{P}_\alpha$ . We find that the optimal sensitivity is obtained by the projective measurement  $\hat{P}_{\pi/2} = |+\rangle\langle+|$  with  $|+\rangle = \frac{1}{\sqrt{2}}(|0\rangle + | -1 \rangle)$ , where

$$\begin{aligned} \langle \hat{P}_{\pi/2} \rangle &= \frac{1}{2} (1 - \cos \beta \sin \theta) \\ \Delta \hat{P}_{\pi/2} &= \sqrt{\langle \hat{P}_{\pi/2}^2 \rangle - \langle \hat{P}_{\pi/2} \rangle^2} = \frac{1}{2} \sqrt{1 - (\cos \beta \sin \theta)^2}, \end{aligned} \quad (\text{S.23})$$

which gives the optimal measurement sensitivity as follows

$$\delta \beta = \frac{\sqrt{1 - (\cos \beta \sin \theta)^2}}{|\sin \beta \sin \theta|}. \quad (\text{S.24})$$

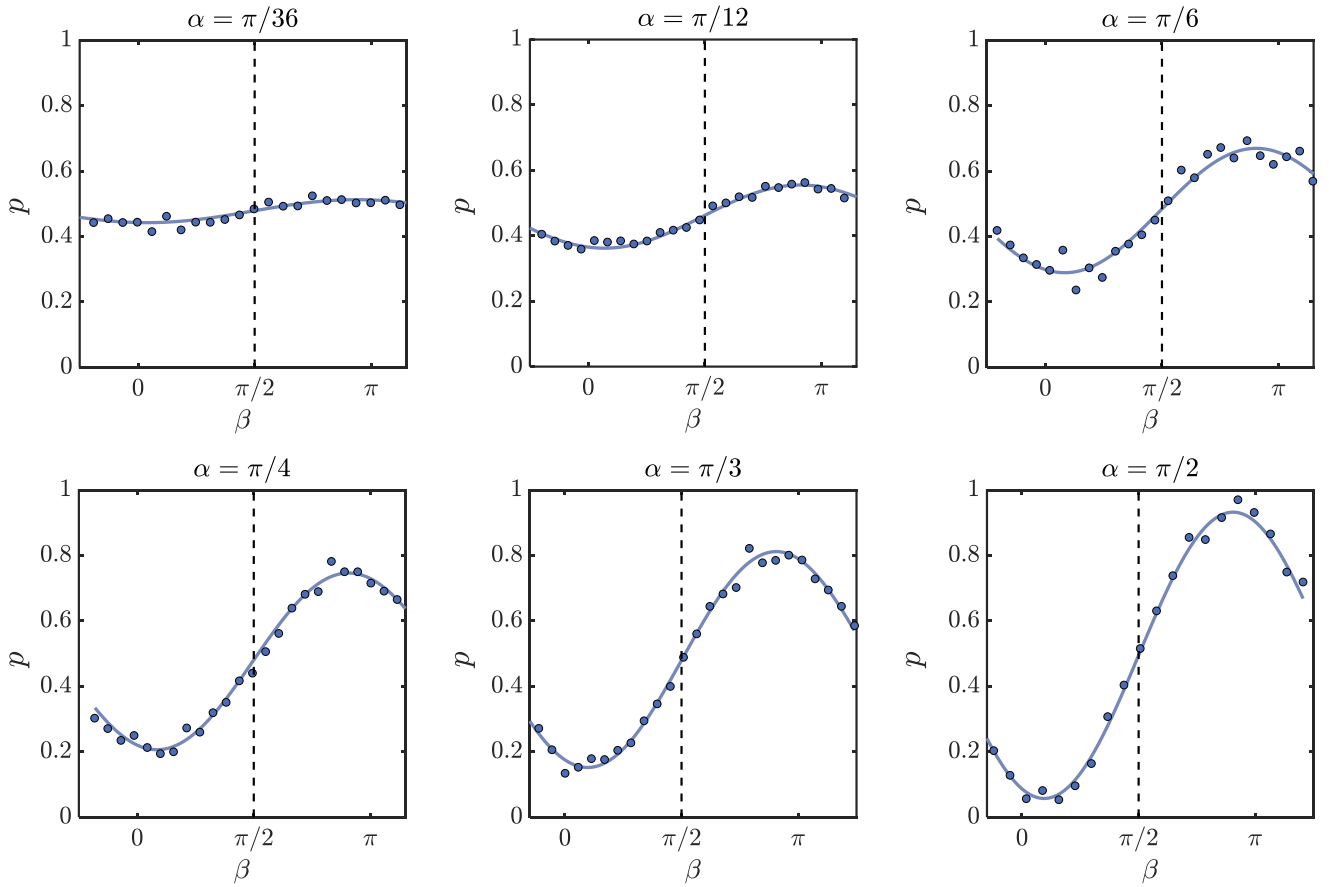


FIG. S5. Parameter estimation with different projective measurements. The measurement signal  $p = \langle \hat{P}_\alpha \rangle$  from the projective measurement  $\hat{P}_\alpha = |\phi_\alpha\rangle\langle\phi_\alpha|$  with  $|\phi_\alpha\rangle = \cos(\alpha/2)|0\rangle + \sin(\alpha/2)|-1\rangle$  is shown as a function of the phase parameter  $\beta$ . The projective measurement  $\hat{P}_{\pi/2}$  leads to the maximum signal contrast, see panel (f), which enables us to achieve the optimum measurement sensitivity for the estimation of the parameter  $\beta$ . The parameter is  $\theta = \pi/2$ .

We set the free evolution time such that the parameter  $\beta = \Delta T$  is close to the working point with the maximum slope of the measurement signal, namely  $\beta \simeq (k \pm 1/2)\pi$ . In this case, the optimal measurement sensitivity (Eq.S.24) can be written as

$$\delta\beta|_{\beta=\frac{\pi}{2}} = \sin^{-1} \theta, \quad (\text{S.25})$$

which equals to  $1/\sqrt{\mathcal{F}_\beta}$ . We note that the QFI is  $\mathcal{F}_\beta = \sin^2 \theta$ . Therefore, by the projective measurement  $\hat{P}_{\pi/2} = |+\rangle\langle+|$  with  $|+\rangle = \frac{1}{\sqrt{2}}(|0\rangle + |1\rangle)$  we achieve the sensitivity limit and verify its connection with quantum Cramér-Rao bound, see Fig.3(d) in the main text.

---

[1] H. Cramér, *Mathematical Methods of Statistics* (Princeton University Press, Princeton, 1946).

[2] C. R. Rao, Information and the Accuracy Attainable in the Estimation of Statistical Parameters, in *Breakthroughs in Statistics: Foundations and Basic Theory* (Springer, New York, 1992) pp. 235–247.

[3] T. Ozawa and N. Goldman, Extracting the quantum metric tensor through periodic driving, *Phys. Rev. B* **97**, 201117 (2018).

[4] M. Yu, P.-C. Yang, M.-S. Gong, Q.-Y. Cao, Q.-Y. Lu, H.-B. Liu, M. B. Plenio, F. Jelezko, T. Ozawa, N. Goldman, S.-L. Zhang, and J.-M. Cai, Experimental measurement of the complete quantum geometry of a solid-state spin system, *Natl. Sci. Rev.* **7**, 254 (2020).